LOCKHEED MARTIN

Terrain Model-Based STAP

By

D. William Luse and Ronald Kuhler

Document No. 5424-REP-001.00-00

6 May 2002

Prepared for:

Mark Novak
AFRL/SNRT
Radar Signal Processing Branch
26 Electric Parkway
Rome NY 13441-4514

Prepared by:

Lockheed Martin Management & Data Systems -
ISR Systems
P.O. Box 85
Litchfield Park, Arizona 85340-0085

Terrain Model-Based STAP

D. William Luse and Ronald J. Kuhler

***Abstract*— The performance of clutter-cancellation GMTI (Ground Moving Target Indication) radar can suffer when observing uneven terrain when the array phase centers are not aligned with the radar vehicle's velocity vector. This type of phase center misalignment is present in a number of existing and proposed GMTI systems. A method for mitigating this problem using a DEM (Digital Elevation Model) for the terrain is described and demonstrated in this paper. The DEM is incorporated into the radar data in such a way that the non-stationarity caused by hilly terrain is greatly reduced, thus allowing reduced-order STAP (Space-Time Adaptive Processing) to be applied.**

***Index Terms*— STAP, GMTI, radar processing, Digital Elevation Model.**

I. Introduction

Most existing and planned airborne multiple-phase-center radars used for Ground Moving Target Indication (GMTI) suffer performance degradation while searching hilly terrain. The problems occur in endo-clutter operation when the phase centers are not aligned with the collection platform's velocity vector. One can view the GMTI operation of such a radar as comparing the Doppler cone angle of return echoes with the angle as measured by interferometric means. Returns for which these two measurements differ are detected as moving targets. The presence of hilly terrain causes unintentional vertical interferometry that corrupts this comparison process. One obvious solution to this problem is to align the phase centers with the platform velocity vector for endo-clutter operation, but the angle of the array base with respect to level varies with the aircraft speed and fuel load. This could be corrected using additional gimbals, but additional leveling gimbals and associated control systems add to system size, weight, cost, and maintenance.

The severity of corruption depends partially upon the particular algorithm being used. The Adaptive Differential Synthetic Aperture Radar (ADSAR) approach for GMTI has been used with great success at the authors' organization for more than nine years on various programs. Although ADSAR is better described as an approach rather than a single algorithm, all implementations have some common features, including identifying the low-order channel-to-channel behavior of the clutter after range and Doppler compression. This model-matching process allows many clutter cells to contribute to the identification of a small number of parameters. In the presence of hilly terrain, this low-order assumption is no longer valid.

This paper presents results demonstrating that the ADSAR approach can be used at close range in hilly terrain with suitable incorporation of DEM data into the processing.

Manuscript received May 7, 2003. This work was supported by DARPA/SPO under contract number F30602-02-C-0037.

The authors are with Lockheed Martin Management and Data Systems-ISR Systems, P.O. Box 85, Litchfield Park, AZ 85340-0085. (e-mails: douglas.w.luse@lmco.com and ronald.j.kuhler@lmco.com).

II. ADSAR Overview

Full order STAP approaches, as described in e.g. [1] require the manipulation of very large covariance matrices. Problems often arise in practical application of full order methods because accurately estimating large covariance matrices requires many samples for averaging. These samples may not be available because of lack of stationarity of the data. Various factored and reduced-rank approaches have been suggested [1]-[3] to reduce the sample covariance size and reduce stationarity requirements. The ADSAR approach reduces the size of the sample covariance matrices to N×N, where N is the number of channels. The ADSAR approach is related to the well-known technique of array calibration on clutter and is probably used in some form at other radar system houses. The underlying requirement for this to work is that certain non-stationary properties of the data obey low-order relationships over range and Doppler. Stated mathematically, let range- and Doppler- compressed complex radar data for N channels be expressed as a three-dimensional data cube:

$x(r,d,c)$, where

$1 \le r \le L$ = number of range samples

$1 \le d \le M$ = number of Doppler samples

$1 \le c \le N$ = number of radar channels

It is assumed that the pulse repetition frequency (PRF) is such that the data for each channel is an unambiguously sampled range-Doppler map of the ground clutter. The channels are assumed to be nominally identical with a certain amount of imbalance in phase and amplitude that may vary with range and Doppler. There is no assumption that the channel phase centers are physically aligned in any particular way.

If two channels, say 1 and 2, are considered, then the low-order assumption means that, for clutter-containing pixels,

$$x(r,d,2) \cong x(r,d,1)a(r,d)e^{j\phi(r,d)} \quad (1)$$

where a and φ are low order polynomials.

The ≅ symbol appears in (1) because the relationship only

holds in a statistical fashion with considerable corruption by noise and other sources of error, though it is assumed to be accurate for the clutter energy. The relationship (1) is generally the case for most practical systems, with the order of the polynomials equal to 1 or 2. At far ranges, the phase difference between channels is approximately linear in range and Doppler because the angle of arrival, of energy returned from the ground, with respect to the axis of any pair of phase centers is nearly linear with range and Doppler. At close ranges, the variation of vertical angle of arrival with Doppler is approximately quadratic. If the channel elements are all fabricated in the same manner with single main lobe patterns, then a small difference in element beam pointing will cause a linear variation of amplitude between the two channel images.

The low order polynomials in (1) have both deterministic and unknown portions. The ADSAR approach is to initially process the data so that the polynomials are as close to unit constants as possible given collection geometry information. One way to do this is to perform SAR processing on each channel with each channel sampled to a complex image on the same output grid and using the same synthetic aperture. For long coherent dwells, it is necessary to perform full SAR processing on each channel. With the shorter dwells used for GMTI, it is generally possible to use a simplified version of SAR processing. This is the motivation for the name ADSAR. The residual differences between channels are then identified using statistical processes. By assumption, these differences are described by low-order polynomials.

In the version of ADSAR used for the data described in this paper, additional channel balance was performed in the transform domain. Specifically, imbalances changing with range frequency (proportional to radio frequency) were identified by averaging over slow time.

III. RADAR DATA

The radar data for this demonstration were collected by the Tuxedo aircraft. This aircraft is a company and government asset of Lockheed Martin M&DS-ISR Systems.

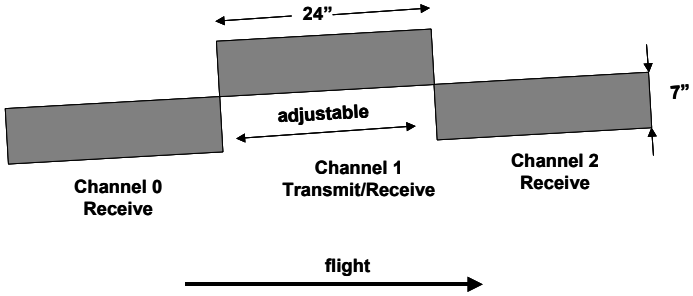

Fig. 1. The Tuxedo aircraft radar has three channels. The locations of the outer phase centers are adjustable.

The Tuxedo radar system has been used for many experiments and demonstrations in recent years. This radar can use a number of different waveforms with a transmit bandwidth limit of 600 MHz and up to 5% duty cycle. Depression angles can range between 10° and 40°. The squint limit is ±8.5°. The following are the particular parameters for the data described in this paper.

Center frequency: 9.6 GHz
Transmit pulse envelope: 100 MHz chirp
Pulse length: 35 microseconds
PRF: 1114.8 Hz
Nominal channel spacing: 2 ft physical
Inter-pulse distance: 0.408 ft
Range = 11.18 nautical miles
Grazing angle: 18.5°
Processed pulses: 512

The region of the collect is the Point of Rocks or Jordan Narrows area on Interstate 15 near Provo, Utah. This area has great diversity of both man-made and natural clutter with considerable topographic relief. Fig. 2 shows a map of the area. An aerial photograph is shown in Fig. 3.

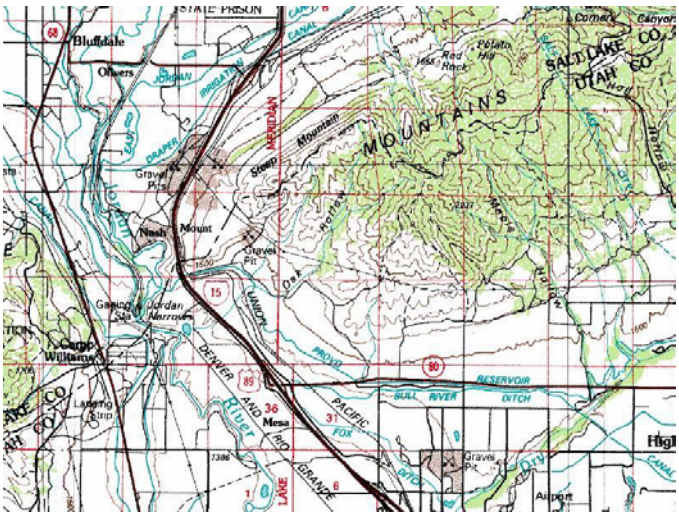

Fig. 2. This map of the Jordan Narrows area indicates topographic relief.

Fig. 3. This aerial photograph shows a mixture of natural, rural, and suburban terrain.

The collected radar range-Doppler image of Fig. 4 clearly shows many of the features visible in the photograph and map.

Many moving target signatures are also visible in the shadows and at the edges of the beam.

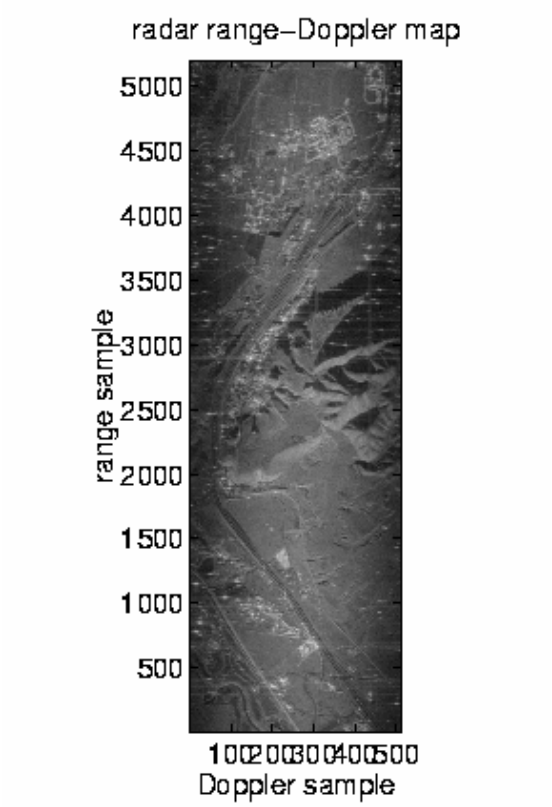

Fig. 4. This radar range-Doppler map has range sample spacing of 4.94 ft and center-image azimuth sample spacing of 16.67 ft.

All three channels yield detected images nearly identical to that shown in Fig. 4 because the amplitude imbalance is minimal. After ADSAR processing, MTI can be performed by simply subtracting pairs of channels. Subtracting the outer two channels yields the greatest sensitivity to radial speed. The outer difference, however, has blind speeds at approximately 12 ft/s as shown in Fig. 5.

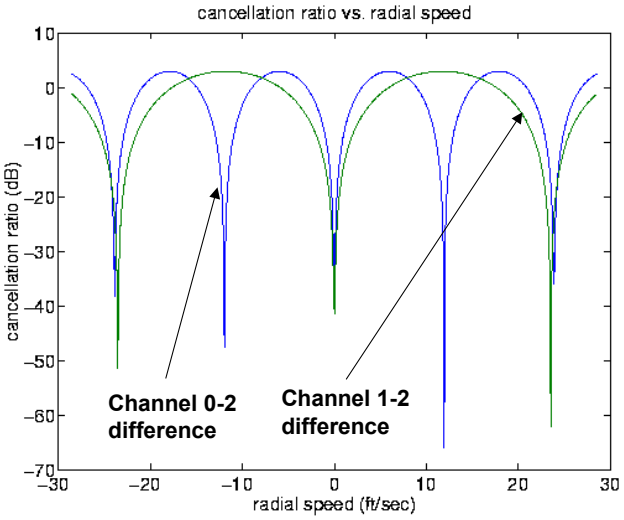

Fig. 5. Plots of cancellation ratio versus radial speed. For practical purposes, only two different sets of weights need be applied for finding moving targets in this three-channel configuration.

If one wants to retain this maximum sensitivity to low speed, the outer difference should be used for primary moving target detection. An additional test on the 1-2 difference (or the 0-1 difference) using a relatively high threshold removes the blind speed at 12 ft/s. Because of the near-symmetric arrangement of the phase centers, there is a blind speed at approximately 23 ft/s no matter what set of weights is used.

IV. DIGITAL ELEVATION MODEL (DEM) DATA

The DEM data for this demonstration was obtained from the United States Geological Survey (USGS) in a government format called Spatial Data Transfer Standard (SDTS). An inexpensive utility called Global Mapper (produced by Global Mapper Software) for viewing and exporting these files is available through internet download sales. Two SDTS products were needed to cover the entire area of the radar collection: Midvale, UT and Jordan Narrows, UT. Both of these have nominal 10 m post spacing. Fig 6 shows an image of the DEM created by the Global Mapper program. The rectangle shows the approximate area of the radar collection.

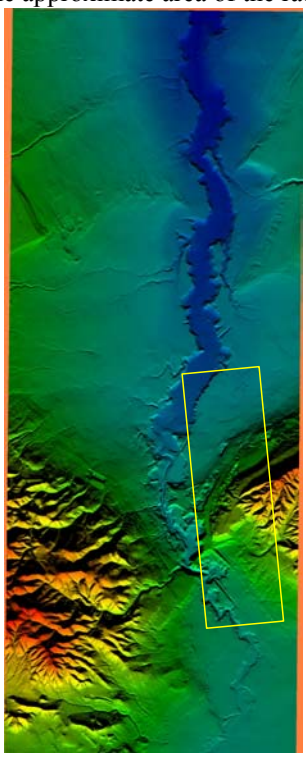

Fig. 6. This image shows two adjacent SDTS products, as rendered by the Global Mapper program.

The association of pixels on a range-Doppler image is easy in principle, but considerable manipulation is necessary for converting standard DEM data to a form suitable for radar calculations. The Global Mapper utility was used to create ASCII files of Cartesian triples from the SDTS data. Although these files are nominally on 10 m posts, there are holes in the data and the post spacing is not consistent. The approach taken here was to resample the DEM data onto an exact 10 m grid using features built into the Matlab (The MathWorks, Inc.) package. The result of this resampling

process is shown in Fig. 7.

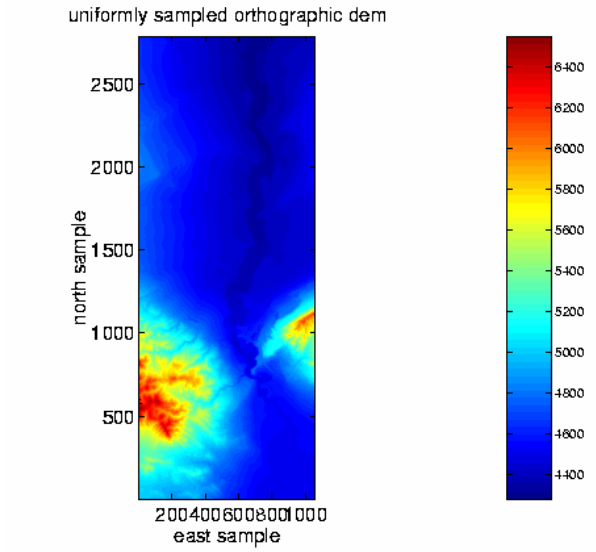

Fig. 7. For convenience in processing, the DEM is resampled to fixed 10 m post spacing.

Using aircraft motion data, each range-Doppler pixel in Fig. 4 is identified with a range-Doppler circle in space. Each range-Doppler circle intersects the DEM at one or more points. There is usually only one intersection point within the beam illumination area. In this way, each range-Doppler pixel is associated with a point in three-dimensional space. The range-Doppler computations were performed here by transforming the aircraft motion data into DEM coordinates. This approach avoids rotating the entire DEM. The result of identifying range-Doppler pixels with DEM coordinates is shown in Fig. 8.

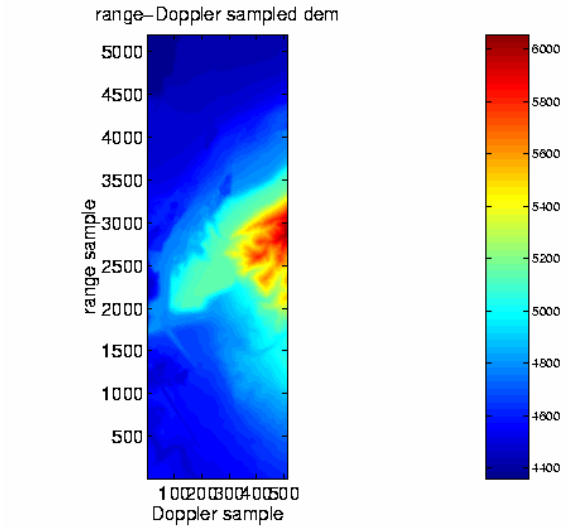

Fig. 8. Map of the "z" component of the Cartesian triple for each range-Doppler cell.

After the intersection of each range-Doppler circle with the DEM has been computed, a ray-tracing procedure determines whether or not the terrain shadows the intersection point. This entails searching the line segment from the intersection point to the aircraft position and checking that all intermediate points lie above the DEM. The resulting binary array is a "shadow mask" that is used to mask areas that should not be used for clutter statistics. The shadow mask is compared with the range-Doppler map in Fig. 9.

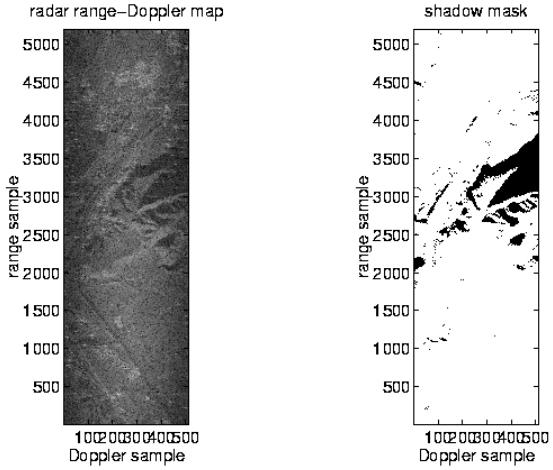

Fig. 9. The shadow mask indicates areas expected to be shadowed based upon DEM computations.

V. PROCESSING RESULTS

The association of range-Doppler pixels with DEM points allows the channel images to be pre-compensated in phase based upon interferometric calculations. This can be viewed as an extension of ADSAR because *a priori* information is being used to make the three channel images as alike as possible for stationary clutter. Figs. 10-15 show six cuts through the image showing identified phase and amplitude imbalance.

These figures show all identified imbalance information. They do not indicate which statistics are used in computing the correction polynomials or how they are weighted in the fitting process. The statistics become inconsistent at the extremes of Doppler because of beam roll-off, as indicated by Figs. 10-13. Shadow areas are evident as inconsistent spikes in the range cuts shown in Figs. 14-15. These inconsistent areas are eliminated in the processing through a combination of adaptive processing and *a priori* knowledge.

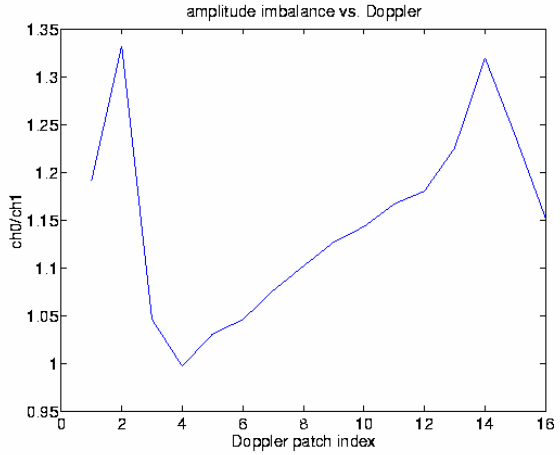

Fig. 10. Identified amplitude imbalance for 0-1 channel pair versus Doppler patch at center range.

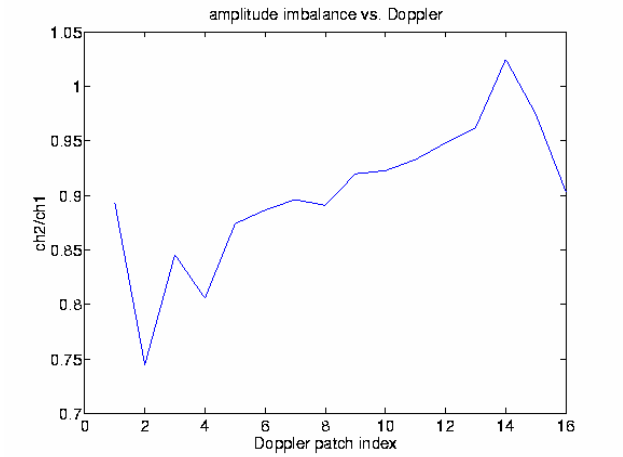

Fig. 11. Identified amplitude imbalance for 2-1 channel pair versus Doppler patch at center range.

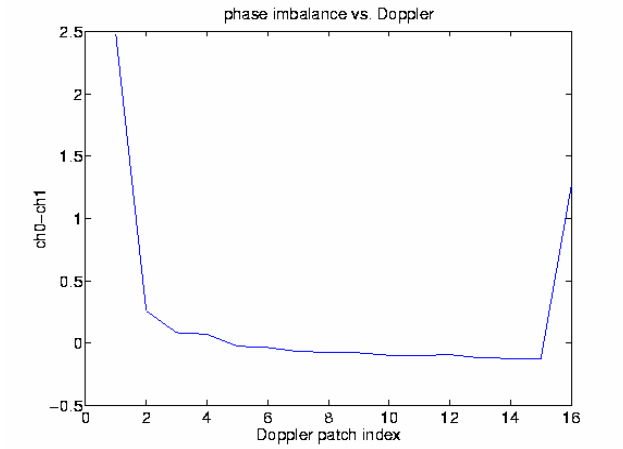

Fig. 12. Identified phase imbalance for 0-1 channel pair versus Doppler patch at center range.

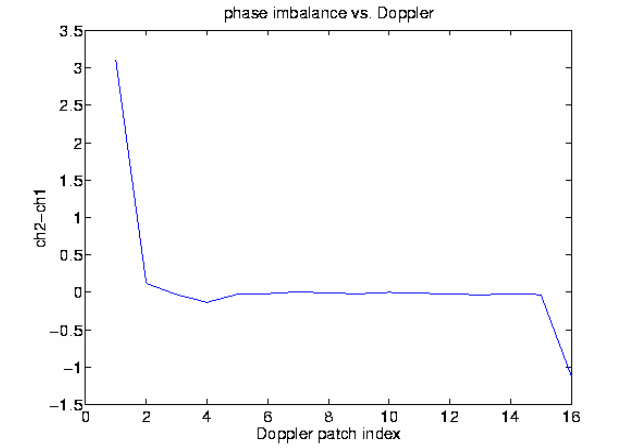

Fig. 13. Identified phase imbalance for 2-1 channel pair versus Doppler patch at center range.

The shadow mask is used to eliminate areas that are expected to be in shadow. This is done by setting their fitting weights to zero. Two patch metrics are computed from the data. These are the square root of the largest eigenvalue and the ratio of the largest to second-largest eigenvalue. A range cut of the largest eigenvalue is shown in Fig. 16. The eigenvalue ratio for the same cut is shown in Fig. 17. A small eigenvalue ratio indicates that there is not a single dominant eigenvalue. This, in turn, means that the clutter in the patch is either near the noise level or it is corrupted by moving target or ambiguous energy.

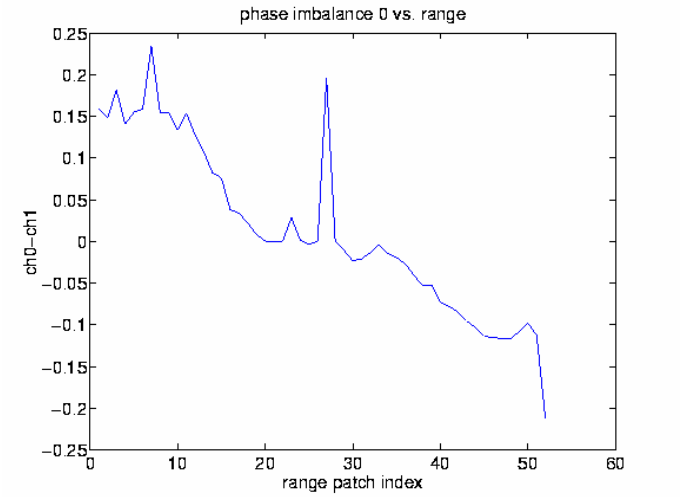

Fig. 14. Identified phase imbalance for 0-1 channel pair versus range patch at center Doppler.

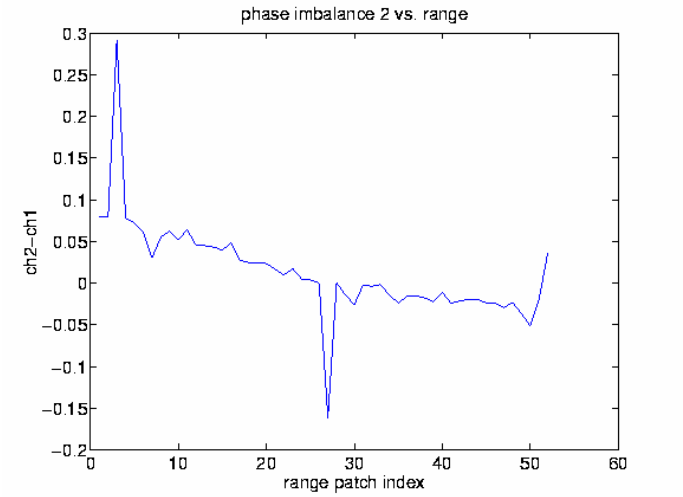

Fig. 15. Identified phase imbalance for 2-1 channel pair versus range patch at center Doppler.

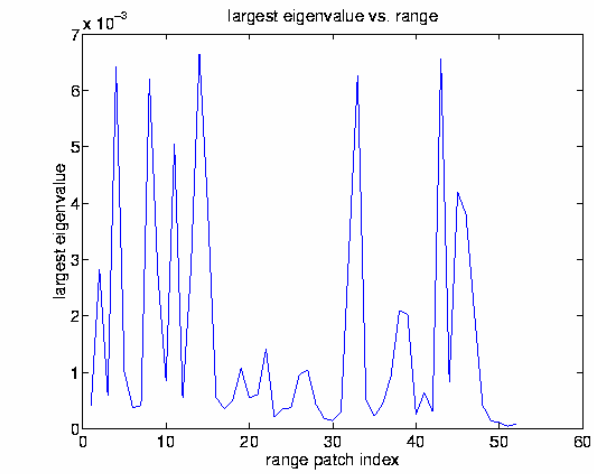

Fig. 16. Largest patch covariance eigenvalue versus range patch at center Doppler.

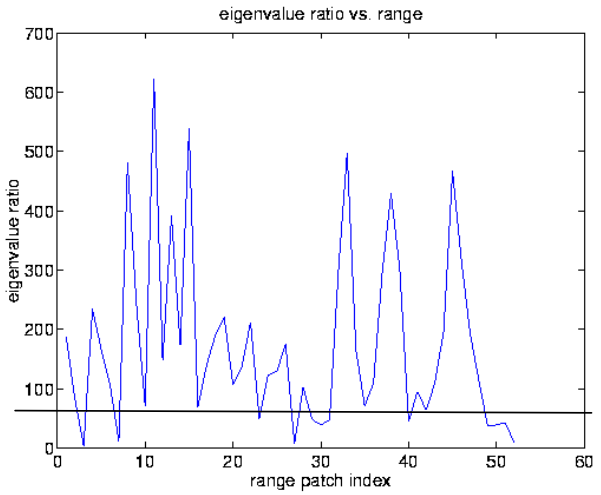

Fig. 17. Eigenvalue ratio versus range patch at center Doppler. The horizontal line shows the rejection level used for this demonstration.

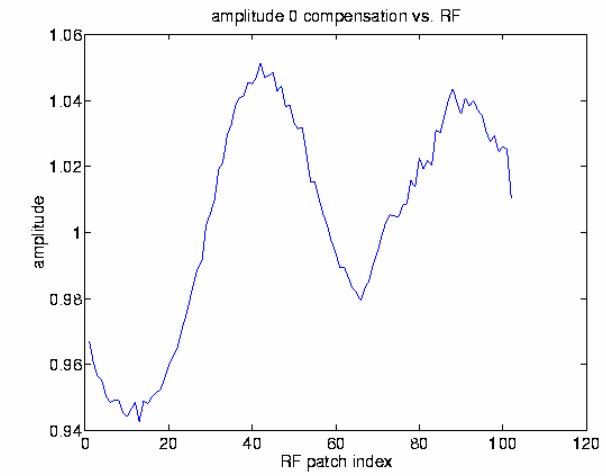

Fig. 18. Identified RF amplitude imbalance correction for the channel 0-1 pair.

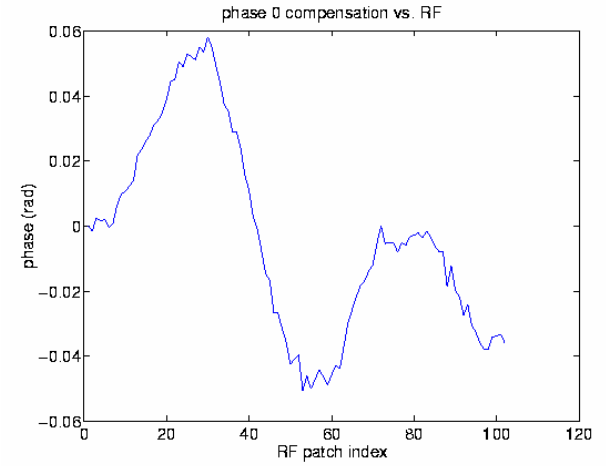

Fig. 19. Identified RF phase imbalance correction for the channel 0-1 pair.

Once the imbalance polynomials are determined, they are used to make phase and amplitude corrections to the images for channels 0 and 2. The images are then back-transformed to the slow-time/RF domain for balancing in RF. Although the imbalances do not fit a low-order model in RF, they are expected to be constant over the short slow-time interval of the data collection. For this reason, a simple averaging over slow time is performed for the RF imbalances. The averaged result for the channel 0-1 pair is shown in Figs. 18-19. The ripple is caused by differences in the filters used for each channel. This RF balance process eliminates the need for using cross-pixel covariance terms as in [3].

After the channels are balanced, difference images are formed. For this demonstration, detection was performed using a simple one-per-million false alarm rate threshold comparison. Pictorial results of this are shown in Fig. 20. The only false alarm rejection technique used was a cancellation ratio test. Each detection pixel is tested by a comparison of pre- and post-cancellation amplitudes. If the cancellation ratio is greater than 20 dB, the detection is rejected. In view of Fig. 5, the minimum detectable velocity imposed by this test is less than one ft/s.

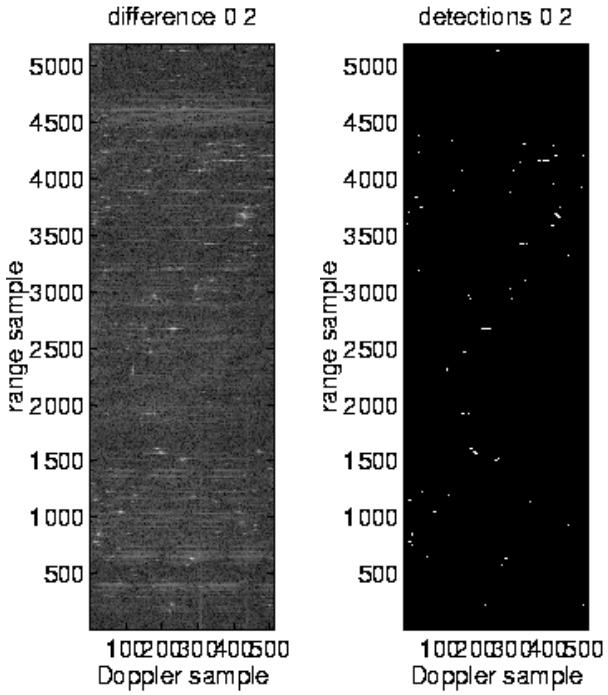

Fig. 20. Difference image and detection map for the 0-2 channel pair.

VI. PERFORMANCE IMPROVEMENT

This section addresses the question of how much GMTI performance is improved by using DEM data in the processing. We start by indicating the magnitude of the phase corrections that result from use of the DEM. Figs. 21-22 show the identified phase imbalances when the DEM is replaced by a flat surface. These are compared to Fig. 23, which is the change in computed grazing angle with and without using the DEM data. This shows that the vertical interferometry shows up clearly in the identified data.

Directly counting detections and false alarms is not practical because there is no ground truth. This is a common problem with testing GMTI systems because ground truth is not practical for large numbers of moving targets.

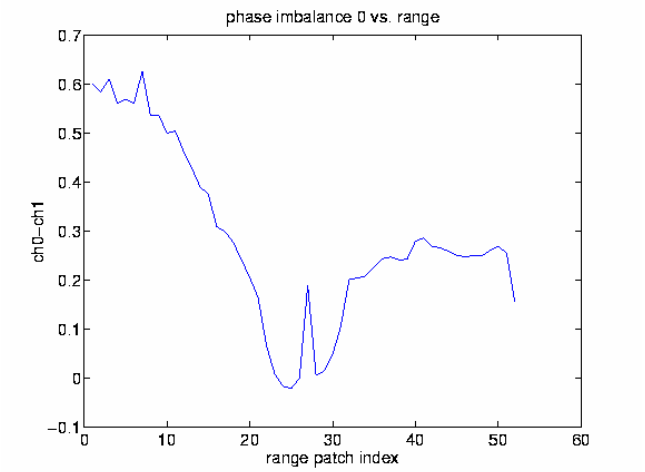

Fig. 21. Identified phase imbalance for the 0-1 channel pair versus range patch at center Doppler without using DEM data.

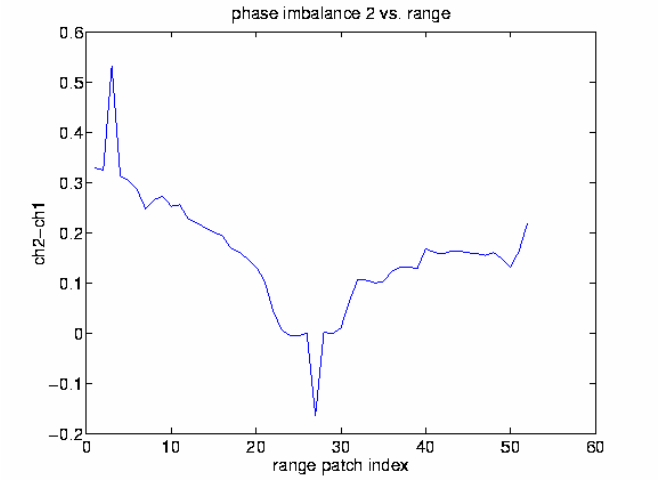

Fig. 22. Identified phase imbalance for the 2-1 channel pair versus range patch at center Doppler without using DEM data.

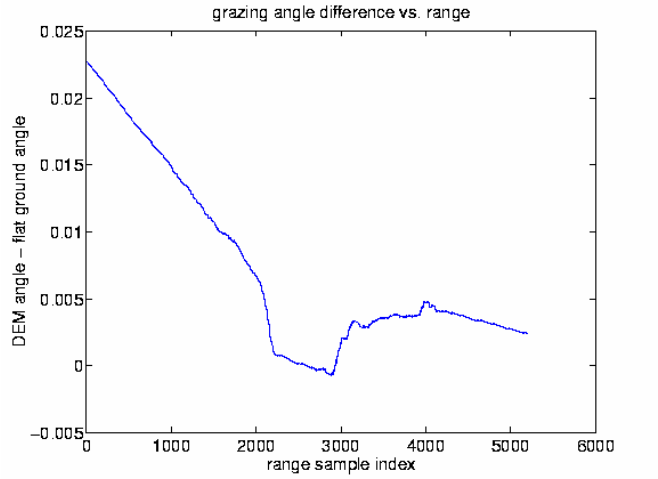

Fig. 23. Grazing angle difference versus range sample. This is the difference in computed grazing angle between the actual DEM and a flat DEM.

Some qualitative techniques, however, are available. One such technique is graphing the cancellation ratio versus pixel amplitude. One expects the low-amplitude pixels to cancel poorly while those with large amplitudes should exhibit high cancellation. Figs. 24-25 show the results with and without DEM inclusion. Although the large number of moving targets leads to choppy graphs, it is apparent that the stronger targets are canceling by several dB more when DEM data are used.

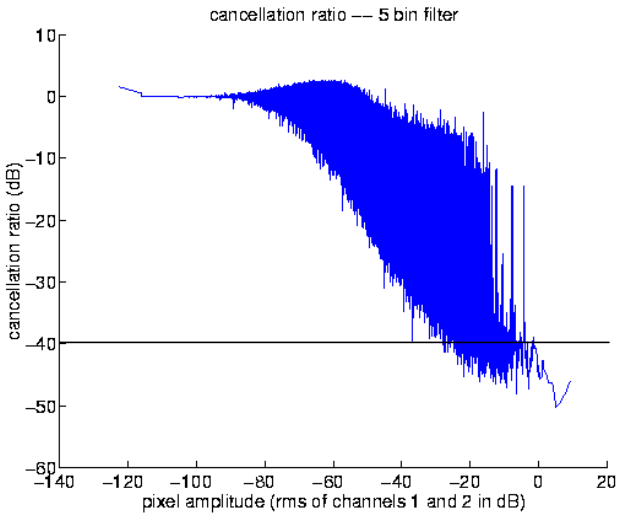

Fig. 24. Cancellation ratio plot using the true DEM.

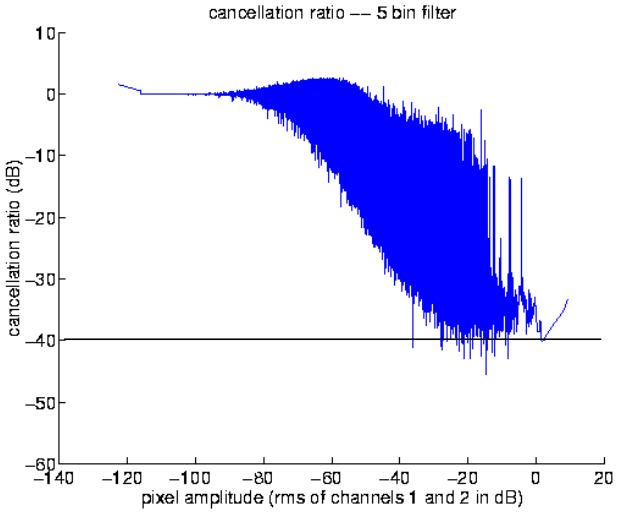

Fig. 25. Cancellation ratio plot using a flat DEM.

A more dramatic indication of improvement is seen by creating the scattergrams of Figs. 26-27. These are created by dividing the complex value of channel 0 (after channel balance) by a complex unit having the angle of the value of channel 1. If there were nothing but stationary clutter energy in the images, this should make all of the pixels real. It is clear that the clutter spreads off the real axis when DEM data corrections are not used. Fig. 28 is included for interest. This scattergram is similar to those of Figs. 26-27 except that the channel differences are used. Thus, Fig. 28 shows the channel 0-1 difference divided by a complex unit having argument equal to that of the channel 1-2 difference. In this view, targets moving at the same radial speed, or multiple pixels from the same target, appear along the same radial. This view indicates the tremendous number of moving target detection pixels present in the data. There were 7161 detection pixels of which 100 were rejected by the false alarm test.

This section is concluded by noting that the main

performance improvement gain by using DEM data was in removing unintentional vertical interferometry. When the processor was run without using the shadow mask for culling data, no apparent degradation in performance was observed. The shadow mask only rejected an additional 5 out of 832 patches.

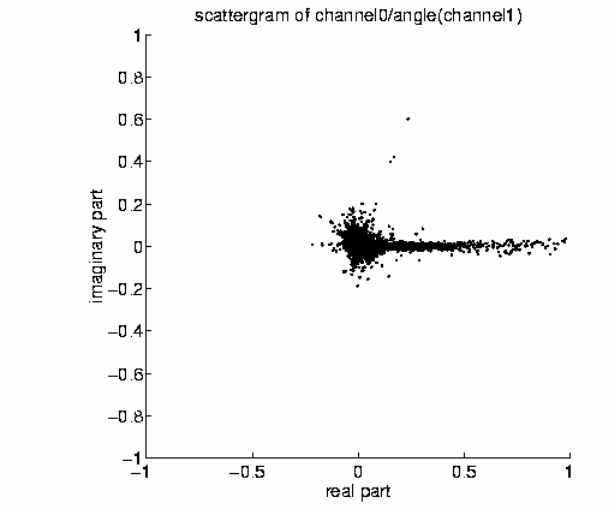

Fig. 26. Scattergram of channel 0 divided by the argument of channel 1 with DEM data included in the processing. The clutter is well concentrated along the real axis.

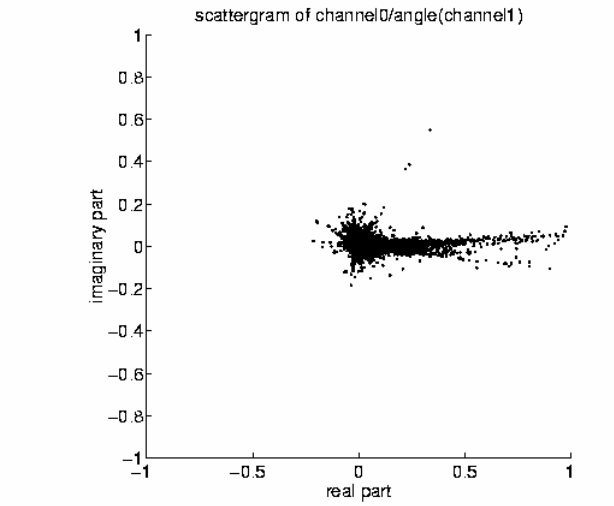

Fig. 27. Scattergram of channel 0 divided by the argument of channel 1 with DEM data not included in the processing. The clutter is spread off of the real axis.

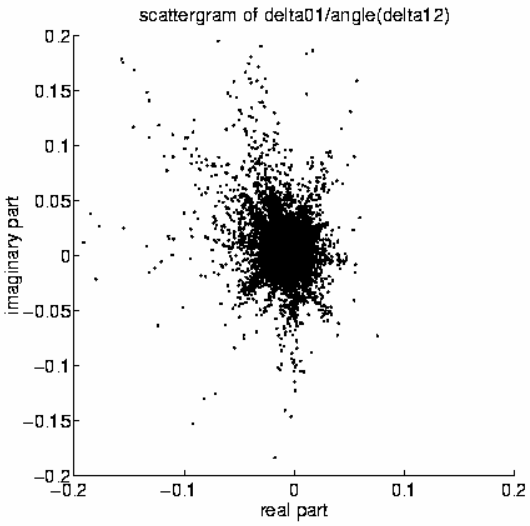

Fig. 28. Scattergram of channel 0-1 difference divided by the argument of the channel 1-2 difference with DEM data included in the processing. Moving targets having the same radial speed appear on the same radial.

VII. CONCLUSION

The conclusion of this paper is that using DEM data can significantly improve the performance of a GMTI processor based upon the ADSAR approach. The DEM information was injected into the processor in two different ways – removing vertical interferometry and predicting shadow areas. It turned out that the processor was very good at eliminating shadows by itself without using *a priori* knowledge. Most or all of the performance gains where attained by making DEM-based phase corrections. The shadow information could still be useful, and possibly even essential, for an operational system. One of the major difficulties of making the approach of this paper operational would be ensuring the quality of the DEM data. A comparison of computed and predicted shadows could be used for this purpose. It could also serve for precise alignment of the DEM with the radar image.

REFERENCES

[1] J. Ward, *Space-Time Adaptive Processing for Airborne Radar*, Lincoln Laboratory Report, Massachusetts Institute of Technology, Lexington, MA, Dec. 13, 1994.

[2] J. R. Guerci, J. S. Goldstein, and I. S. Reed, "Optimal and Adaptive Reduced-Rank STAP," *IEEE Trans. On Aerospace and Electronic Systems, Vol. AES-36, No. 2, pp. 647-663, April 2000.*

[3] R. C. DiPietro, "Extended Factored Space-Time Processing for Airborne Radar Systems," *Proc. Twenty-Sixth Asilomar Conference on Signals, Systems and Computers,* 26-28 Oct 1992, pp. 425 -430 vol.1.